

Journal of Climate Change, Vol. 7, No. 3 (2021), pp. 9-21. DOI 10.3233/JCC210015

On the Global Contrasting Temperature-Precipitation Phase Mechanisms in the Last Century

A.P. Dimri*, P. Kumar and P. Maharana

School of Environmental Sciences, Jawaharlal Nehru University, New Delhi, India ⊠ apdimri@hotmail.com

Received November 27, 2020; revised and accepted August 2, 2021

Abstract: Global precipitation patterns have changed compared to the before 1960 (pre-industrial period). By now the temperature has risen by approximately 1°C. The atmospheric heat-retaining constituents have been raised by human-induced activities. It is influencing the composition of the atmospheric gases and water vapour leading to tropospheric energy budget imbalance affecting atmospheric pressure systems. Increased atmospheric warming leads water holding capacity to rise. Such changes insinuated contrasting phases: decreased (increased) temperature- increased (decreased) precipitation in the last century. Mechanisms of these in- and out- phases are investigated. In the total four (two colder-wet and two warmer-dry) global conditions are observed. These time slices indicate a gradual increase in global temperature and a decrease in precipitation. Clausius-Clapeyron relation suggests abrupt warming and increased water vapour pressure in recent decades. In addition, the global climate system is shifting towards abnormal warm-wet or warm-dry conditions. Further, contrasting changes in global precipitation have been seen, in particular after 1960 (post-industrial period). It is significantly noted that there has been a global contrasting temperature-precipitation phase mechanism in the last century.

Keywords: Clausius-Clapeyron; Precipitation; Temperature; Global change; Wet/dry-warm/cold.

Introduction

Human-induced unexpected global warming is a major cause of climate change (Chen and Dai, 2019; Hansen et al., 2006; Trenberth et al., 2003). The global average temperature is on a consistent rise (Hansen et al., 2006, 2010; Trenberth, 2011). The escalation of greenhouse gases concentrations in the atmosphere through anthropogenic agitation led to an imbalance between incoming shortwave radiation and outgoing longwave radiation causing global warming (Cheng et al., 2019; Intergovernmental Panel on Climate Change, 2014; Schuckmann et al., 2016; Trenberth, 2011; Trenberth et al., 2013). The radiation and heat budgets are the key factors in driving the precipitation mechanism that controls atmospheric moisture content (water vapour pressure) as well as surface temperature. The

increased global tropospheric load due to anthropogenic activities also influences the radiation budget of the earth (Rosenfeld et al., 2008). Further, they also act as cloud seeding material leading to precipitation formation (Ramanathan, 2001; Rosenfeld, 2000; Rosenfeld et al., 2008; Trenberth et al., 2003). Few studies advocate that global precipitation changes are controlled by the energy budget (Hegerl et al., 2015; Trenberth, 2011). The rising global temperature enhances the moistureholding capacity of the air parcel by approximately 7% per °C rise in temperature following Clausius-Clyeporan (C-C) relation (Berg et al., 2013; Chen and Dai, 2019; Held and Soden, 2006; Jones et al., 2010; Maeda et al., 2012; Trenberth, 2011; Trenberth et al., 2003). Thus, increasing global temperatures lead to higher precipitation intensity (Maeda et al., 2012). However, this particular assumption does not fit to be perfect all

the time. Global precipitation changes with temperature rise are following 'never or extreme' precipitation pattern. A decrease in the total precipitation trend is reported globally (Berg et al., 2017; Hansen et al., 2010; Trenberth et al., 2003; Trenberth and Zhang, 2018). It is illustrated that the world's land aridity is increasing with decreased soil moisture (Berg et al., 2017). Some studies proposed the global warming and precipitation behaviour closely follow the C-C relation (Allan et al., 2010; Berg et al., 2009, 2013; Haerter et al., 2010; Haerter and Berg, 2009; Lenderink and van Meijgaard, 2008; Liu et al., 2009; Maeda et al., 2012).

Hence, assessment of abrupt changes in temperature-precipitation relationship global scale remains a puzzle. Therefore, the present study investigates the global average temperature-precipitation over landmass during the last century. Out of the four (two colder-wet and two warmer-dry) global conditions are identified (Figure 1). These global conditions are chosen when combined temperature and precipitation are either in or out of the respective phases. Using robust analysis, the associated mechanisms are provided in the present paper.

Data and Methods

This study examines an updated Climate Research Unit (CRU) TS Version 4.02 (Harris et al., 2014) dataset

for the present analysis. The CRU dataset has been constructed using various station data adopting the climate anomaly method (Harris et al., 2014; Peterson et al., 1998) (CAM). Various meteorological variables (e.g., temperature [T], precipitation [P], water vapour pressure [WVP], potential evapotranspiration [PET], maximum and minimum temperature [Tmax and Tmin] and diurnal temperature range [DTR]) are utilised in the present study. These monthly average datasets at 0.5° resolution have been analysed from 1901 to 2017 (Table 1).

The present study proposes a few conditions to identify the period of cold/warm and wet/dry contrasting global changes of temperature-precipitation (CGTPC, hereafter). Firstly, the standardized temperature anomaly (STA, hereafter) and standardised precipitation anomaly (SPA, hereafter) are computed during the study period.

Standardized Anomaly (SA) =
$$\left(\frac{X - \overline{X}}{SD}\right)$$
 (1)

where X = time series, $\overline{X} =$ long-term mean, and SD= standard deviation.

Secondly, the periods of CGTPC are determined where the 'STA \leq -0.2 and corresponding SPA \geq 0.5' or 'STA \geq 0.2 and corresponding SPA \leq -0.5' for at least three consecutive years. Therefore, four time slices for CGTPC identified during the study period are Slice 1

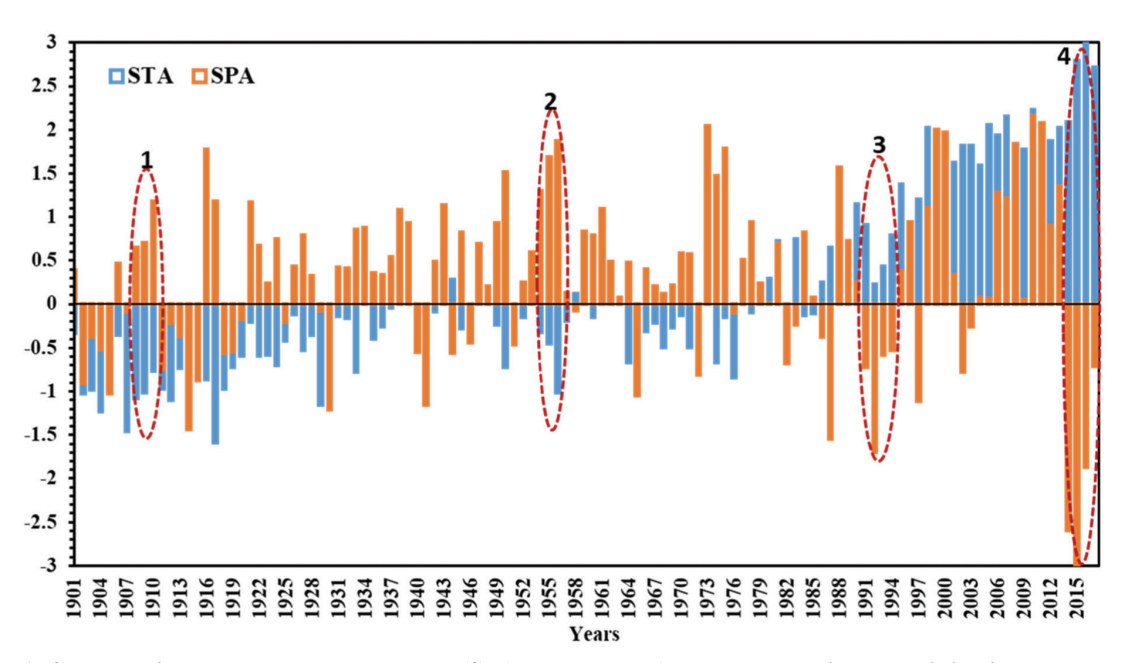


Figure 1: Standardized temperature anomaly (STA: blue colour) and standardized precipitation anomaly (SPA: orange colour) from long-term (1901-2017) average for global landmass. The dot-dot circles represent in- and out- phases in temperature and precipitation for particulars consecutive years (as per the postulate: "At least three continuous years with STA \leq -0.2 and corresponding SPA \geq 0.5 'or' STA \geq 0.2 and corresponding SPA \leq -0.5"). The time slices obtained are: Slice 1 (1908, 1909, 1910), Slice 2 (1954, 1955, 1956), Slice 3 (1991, 1992, 1993, 1994) and Slice 4 (2014, 2015, 2016, 2017).

Study time period

Temporal and Horizontal resolution

Variables

Monthly and 0.5° lat./lon.

temperature (T),
precipitation (P),
water vapour pressure (WVP),
potential evapotranspiration (PET),
maximum temperature (Tmax),
minimum temperature (Tmin),
diurnal temperature range (DTR)

Table 1: CRU TS Version 4.02 Dataset (global land surface) used for the present study

(cold -wet): 1908–1910; Slice 2 (cold-wet):1954–1956; Slice 3 (warm-dry): 1991–1994; Slice 4 (warm-dry): 2014 – 2017 (Figure 1, Tables 2 and 3).

Thereafter, the relationship among T, WVP and P as discussed below are investigated in these respective slices.

The saturation water vapour pressure (P_{ws}: SWVP) is calculated using temperature (Murray, 1967; Osborne and Meyers, 1934)

$$P_{ws} = \exp\left(A + \frac{B}{T} + C \times lnT + DT\right) \tag{2}$$

A=77.34, B=7235, C= -8.2, D= 0.005711, and T = temperature (K)

Percentage change of precipitation (P% change) is computed (Yang Shao-E and Wu Bing-fang, 2010)

$$\Delta P \% = \left(\frac{X - \overline{X}}{\overline{X}}\right) \times 100 \tag{3}$$

Where X = precipitation time series, and $\overline{X} =$ long-term mean of annual precipitation.

Temperature and Precipitation Anomalies

The standardized anomaly (e.g., STA and SPA) provides a justified idea about the relative rarity of events compared to climatology (Grumm and Hart, 2001; Richardson et al., 2018). Apart from considering the entire period from 1901 to 2017 (Figure 2); two subperiods (1901 – 1960: pre-industrial and 1961 – 2017: post-industrial) are also considered to examine the anomalous behaviour of CGTPC. Out of the four slices of CGTPC identified; two events occurred before 1960 and the other two after 1960. Slice 1 (1908 – 1910) and Slice 2 (1954 – 1956) are identified following the criteria of 'STA \leq -0.2 and corresponding SPA \geq 0.5'. However, Slice 3 (1991 – 1994) and Slice 4 (2014 – 2017) are identified based on 'STA ≥ 0.2 and corresponding SPA \leq -0.5' (Figure 1). These four slices of events derived using the SPA and STA suggest abrupt changes in climatic conditions (Figure 1). These slices indicate towards gradual increase (decrease) of the global temperature (precipitation). Interestingly, the CGTPC has become more frequent and intense in recent times (Figure 1). The behaviour of most recent Slices 3 and 4 clearly indicates a rapid anthropogenic influence on the climate system. This leads to a warm and dry global condition in the recent period (Slice 4). The composite of mean temperature during Slice 1 shows an anomalous cooling over the entire landmass (except over East-North America, East and Central Brazil, Mali, Mauritania, and Madagascar at regional scales), which is much intense over Alaska and Russia (Figure 3a). Slice 2 shows a gradual rise in global mean temperature. However, the anomalous cooling still persists over the entire globe (except over the North-East America region, which experiences intense warming) (Figure 3b). During the post-industrial period, the behaviour of CGTPC has completely changed as compared to the earlier slices, which is evident from Slices 3 and 4. This shows that the colder regions in the first two slices (Figure 3a-b) became warmer in later slices (Figure 3c-d). The high-latitude regions (ranging from 45 to 60°N) are found to be the hotspots of climate change as these regions are sensitive to global temperature changes. These regions are expected to be affected more by the impact of climate change as compared to the tropical regions. This behaviour further intensified in Slice 4 (Figure 3d): where the entire globe is anomalously warmer, indicating a rapid increase in global temperature (Hansen et al., 2006). The rapid rise of global temperature in recent times is attributed to the escalation of the anthropogenic emission (Booth et al., 2012), which has also increased relative to longterm temperature climatology (Booth et al., 2012; Chen and Dai, 2019; Hansen et al., 2006; Trenberth, 2011; Trenberth et al., 2003; Trenberth and Zhang, 2018) (Figure 2). The behaviour of precipitation in these slices is different as compared to the corresponding temperature (Figure 3e-h). In Slice 1, the precipitation is

Table 2: Table represents the time slices selected for the study as per the postulate "At least three continuous years with STA \leq -0.2 and corresponding SPA \geq 0.5 or STA \geq 0.2 and corresponding SPA \leq -0.5". The time spans are obtained from the global mean as Slice 1 (1908, 1909, 1910), Slice 2 (1954, 1955, 1956), Slice 3 (1991, 1992, 1993, 1994) and Slice 4 (2014, 2015, 2016, 2017). Where STA and SPA are Standardized Temperature and Anomaly; and Standardized Precipitation Anomaly respectively

Year	STA	SPA	Year	STA	SPA	Year	STA	SPA
1901	-0.3379	0.3931	1940	-0.0797	-0.5495	1979	0.0916	0.2396
1902	-1.0252	-0.9055	1941	-0.0690	-1.1572	1980	0.2963	0.0077
1903	-0.9885	-0.3766	1942	-0.0843	0.4929	1981	0.7267	0.6967
1904	-1.2361	-0.5151	1943	0.0797	1.1381	1982	-0.0503	-0.6769
1905	-0.9072	-1.0245	1944	0.2779	-0.5583	1983	0.7449	-0.2378
1906	-0.3542	0.4625	1945	-0.2794	0.8201	1984	-0.1279	0.8201
1907	-1.4585	-0.0884	1946	-0.1734	-0.4385	1985	-0.1088	0.0745
1908	-1.0846	0.6517	1947	0.0419	0.6968	1986	0.2537	-0.3790
1909	-1.0161	0.7024	1948	0.0283	0.2107	1987	0.6532	-1.5409
1910	-0.7633	1.1854	1949	-0.2339	0.9285	1988	0.8661	1.5735
1911	-0.9672	-0.7486	1950	-0.7234	1.5112	1989	0.5507	0.7237
1912	-1.1006	-0.2168	1951	-0.2313	-0.4640	1990	1.1516	0.2448
1913	-0.7360	-0.3645	1952	-0.1488	0.2520	1991	0.9083	-0.7251
1914	-0.1677	-1.4401	1953	0.3458	0.5956	1992	0.2241	-1.6973
1915	-0.1540	-0.8713	1954	-0.3270	1.2974	1993	0.4386	-0.5778
1916	-0.8618	1.7764	1955	-0.4494	1.6882	1994	0.7960	-0.5303
1917	-1.5880	1.1842	1956	-1.0201	1.8760	1995	1.3762	0.3834
1918	-0.9768	-0.5615	1957	-0.1928	0.1329	1996	0.5552	0.9376
1919	-0.7197	-0.5428	1958	0.1230	-0.0768	1997	1.2017	-1.1087
1920	-0.5986	-0.1676	1959	0.0530	0.8334	1998	2.0194	1.1017
1921	-0.1994	1.1653	1960	-0.1512	0.7887	1999	1.3314	1.9973
1922	-0.5935	0.6710	1961	0.0944	1.0890	2000	1.1530	1.9695
1923	-0.5878	0.2396	1962	0.0663	0.4831	2001	1.6224	0.3340
1924	-0.7022	0.7458	1963	0.0586	0.0740	2002	1.8200	-0.7755
1925	-0.4162	-0.2038	1964	-0.6719	0.4808	2003	1.8144	-0.2540
1926	-0.1194	0.4359	1965	-0.5601	-1.0445	2004	1.5872	0.0737
1927	-0.5340	0.7873	1966	-0.3152	0.3969	2005	2.0534	0.0712
1928	-0.3588	0.3259	1967	-0.2146	0.2086	2006	1.9355	1.2816
1929	-1.1548	-0.0725	1968	-0.4974	0.1208	2007	2.1520	1.2130
1930	-0.2164	-1.2115	1969	-0.2740	0.2167	2008	1.6508	1.8420
1931	-0.1379	0.4244	1970	-0.1248	0.5894	2009	1.7701	0.0549
1932	-0.1629	0.4141	1971	-0.4924	0.5763	2010	2.2275	2.1606
1933	-0.7767	0.8553	1972	-0.5469	-0.8108	2011	1.7699	2.0789
1934	0.00217	0.8792	1973	0.3336	2.0474	2012	1.8686	0.9025
1935	-0.3990	0.3563	1974	-0.6732	1.4675	2013	2.0223	1.3564
1936	-0.2596	0.3361	1975	-0.1548	1.7900	2014	2.0890	-2.5935
1937	-0.0379	0.5367	1976	-0.8434	-0.0975	2015	2.7936	-3.9510
1938	0.42676	1.0782	1977	0.2055	0.5094	2016	3.1304	-1.8710
1939	0.08957	0.9360	1978	-0.1002	0.9422	2017	2.7174	-0.7165

Slices	Precipitation (P)	Temperature (T)
Slice 1	P↑	T ↓
Slice 2	P↑	T ↓
Slice 3	P↓	T ↑
Slice 4	P↓	T↑

Table 3: Global land precipitation and temperature increase (upward arrow) or decrease (downward arrow) for each slice

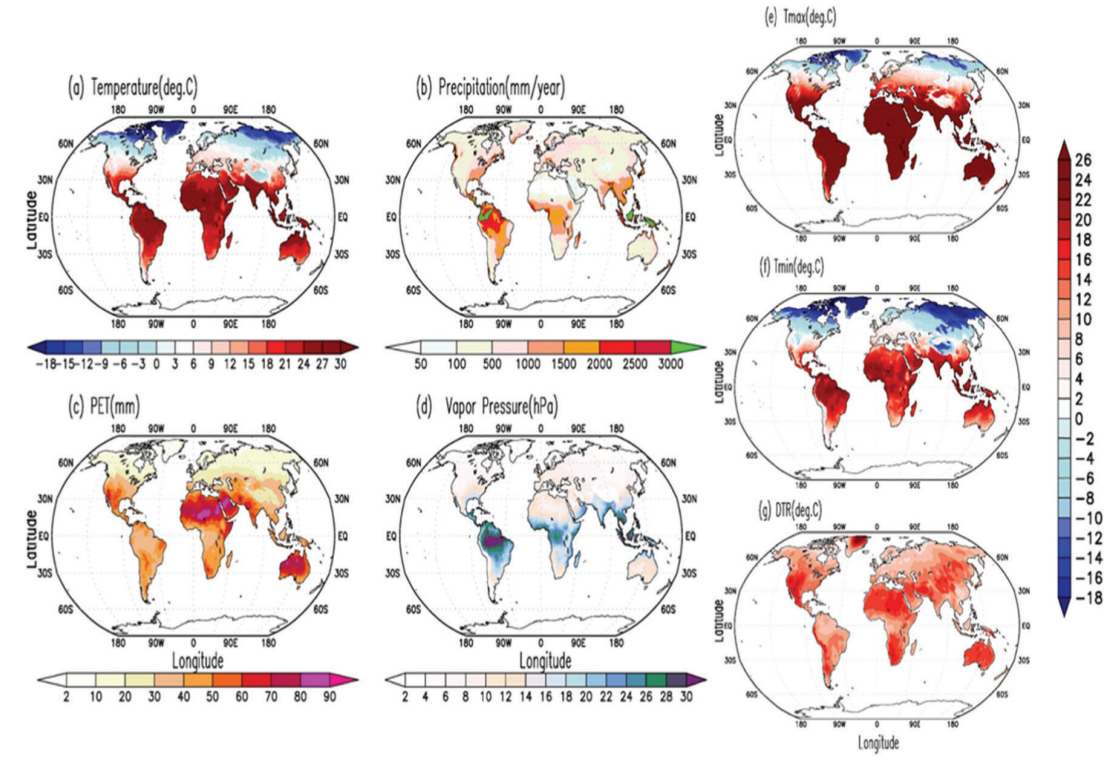


Figure 2: Climatology of the (a) Temperature, (b) Precipitation, (c) Potential Evapotranspiration (PET), (d) Water Vapour Pressure, (e) Maximum Temperature (Tmax), (f) Minimum Temperature (Tmin) and (g) Diurnal Temperature Range (DTR) is shown for long-term (1901 to 2017).

anomalously lower over the higher latitude of Northern Hemisphere (NH) and Argentina in Southern Hemisphere (Dore, 2005) (SH). However, tropical regions receive anomalously higher precipitation (including Australia in SH) (Figure 4). The precipitation further intensifies particularly near the equatorial regions (India, tropical Africa, western Australia and the northern part of South America) during Slice 2 (Figure 3f). With the rapid rise of global temperature, the precipitation shows exactly opposite behaviour and the prominent precipitation peaks particularly around the equatorial regions (Slice 2) showing the sign of rapid drying (Slice 3; Figure 3g). However, precipitation distribution during Slice 4 is very heterogeneous. In which higher anomalous precipitation is observed over the higher latitudes of

both NH and SH (Huffman et al., 2009; Trenberth, 2011). The tropical regions around both the hemispheres (including Colombia, Venezuela, Brazil, African forest region, Senegal, Mali, northeast India and Indonesia) are anomalously dry in the recent times (Dore, 2005; Gu et al., 2007) (Figure 3g,h). Human induced warming achieved approximately 1°C above pre-industrial in 2017 globally (IPCC, 2018). Few researchers illustrated the rapid rate of increase in the daily Tmin as compared to the daily Tmax results in decrease in DTR (Braganza et al., 2004; Caesar et al., 2006; Davy et al., 2016; Easterling et al., 1997; Thorne et al., 2016; Wild et al., 2007; Yang et al., 2013). Following the behaviour of mean temperature, a low anomalous Tmax is observed globally in Slice 1 (except Oklahoma, Texas, Louisiana,

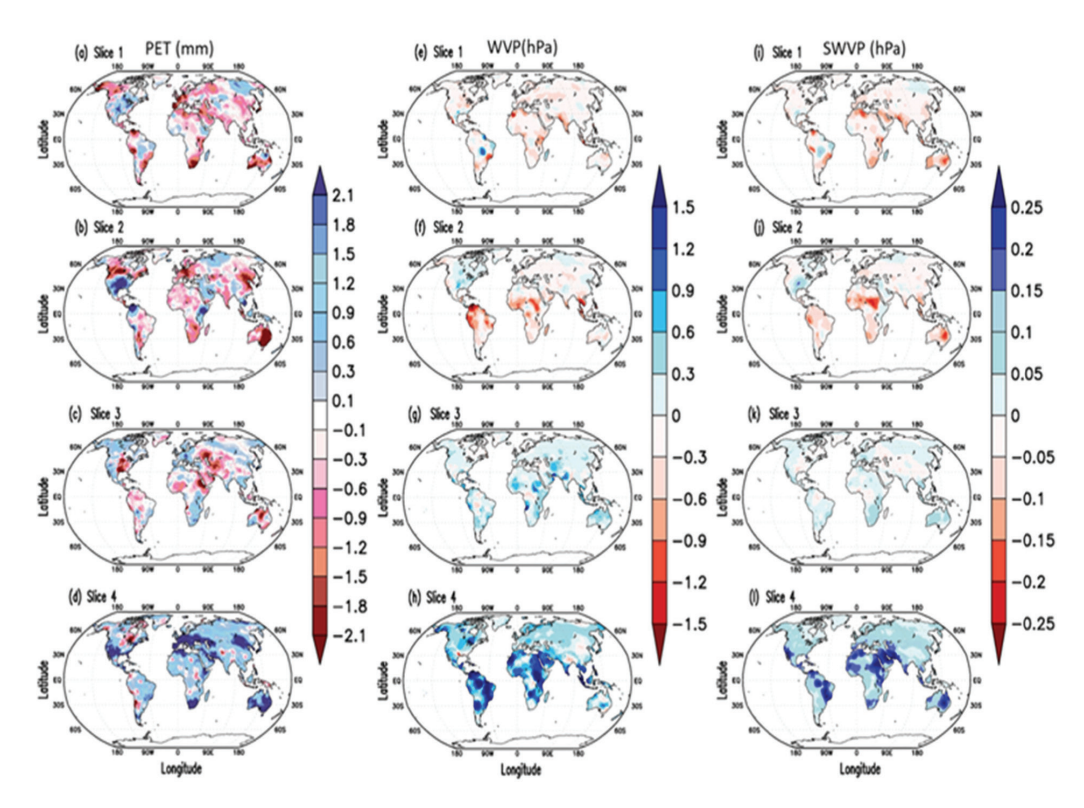


Figure 3: Anomalous change in potential evapotranspiration (PET) (mm) (a-d), water vapour pressure (WVP) (e-h) and saturation water vapour pressure (SWV) (hPa) (i-l) are shown for each time of slices (as composite mean).

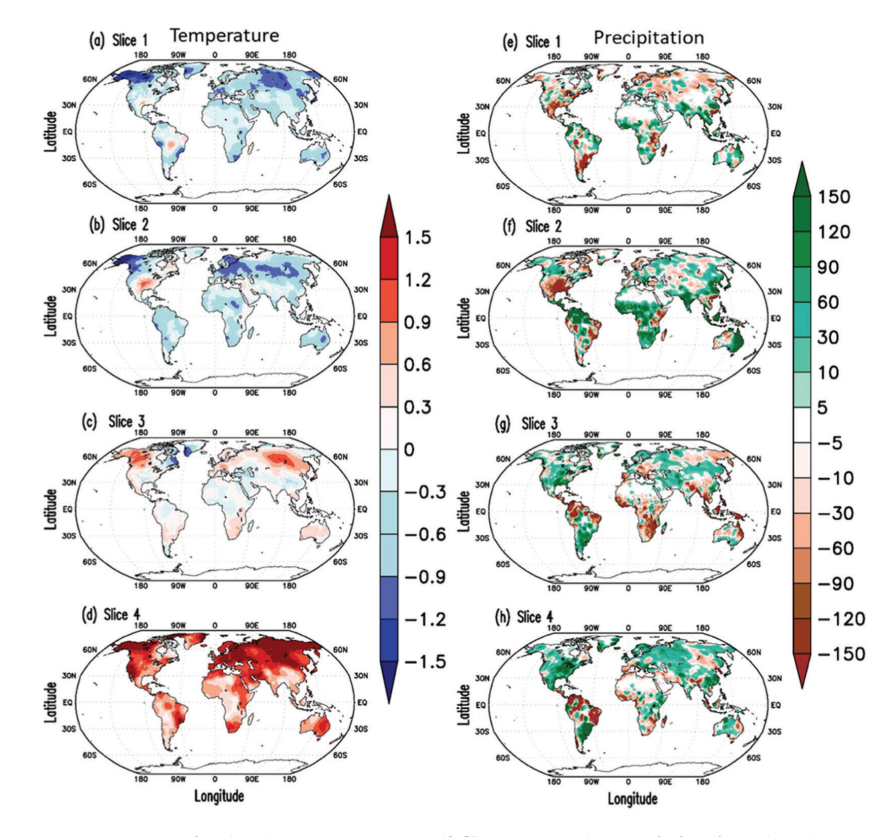


Figure 4: Anomalous change in (a-d) temperature (°C) and (e-h) precipitation (mm) are shown for each time of slices (as composite mean).

Arkansas USA and Western Brazil) (Figure 5a). Slice 2 has almost a similar spatial pattern to Slice 1 with anomalous high Tmax over the eastern US (Figure 5b). During the post-industrial period, a clear transition of extratropical warming compared to tropics is noticed in Slice 3 (Figure 5c). In the recent period, the entire globe experiences anomalous warming ranging from 0.6 to 1.5°C magnitude with relatively higher escalation over the extratropical region (Hansen et al., 2006) in Slice 4 (Figure 5d). The Tmin anomaly also follows a similar pattern to the Tmax in all four slices (Figure 5e-h). The transition of DTR anomaly from positive to negative change from Slice 1 to 4 indicates an anomalous rise of nighttime temperature (or Tmin) except over North America, South Africa, Australia and Europe (Thorne et al., 2016) (Figure 5i-l). The DTR pattern further helps to explain clouds, precipitation, soil moisture, the planetary boundary layer (PBL) and other feedback processes as well (Davy et al., 2016; Thorne et al., 2016). In addition, the intense anomalous positive nighttime (minimum) temperature is observed in Slice 4 (Figure 5h). This indicates climate change-induced anomalous higher night-time temperature compared to Tmax (Davy et al., 2016; Easterling et al., 1997; Karl et al., 1991).

Discussions

The potential evapotranspiration (PET) is estimated

using temperature and day duration (Ahn and Tateishi, 1994; Lu et al., 2005; Palutikof et al., 1994; Tsakiris and Vangelis, 2005). The rise in global mean surface air temperature by 1°C from the pre-industrial period is also changing the scenario of precipitation distribution. This indicates a shift in moisture availability due to increased anthropogenic activity (Ahn and Tateishi, 1994; Palutikof et al., 1994). PET is the available amount of moisture to evaporate from land (Scheff and Frierson, 2014) (e.g., water demand). Anomalous low PET corresponding to Slice 1 and 2 suggests low precipitation (Figure 3a and b) and strong wind circulation (Shenbin et al., 2006). However, an anomalous increase in PET indicates rising aridity and drought (Slice 3 and 4) (Figure 3c and d) through human-induced warming (Scheff and Frierson, 2014). The gradual global temperature rise increases the water holding capacity of the atmospheric column (following C-C relation). This leads to the increase in the water vapour pressure during the post-industrial period (higher values in Slice 3 and 4) as compared to the pre-industrial period (Trenberth, 2011) (lesser values in Slice 1 and 2)(Figure 3e-h). The weather and climate variability depend on the changed pressure systems. As energy flows from high to low-pressure system, it invokes synoptic to mesoscales weather systems. Water vapour is mainly responsible for the atmospheric pressure variation. That is why the water vapour pressure (WVP) and saturated water vapour

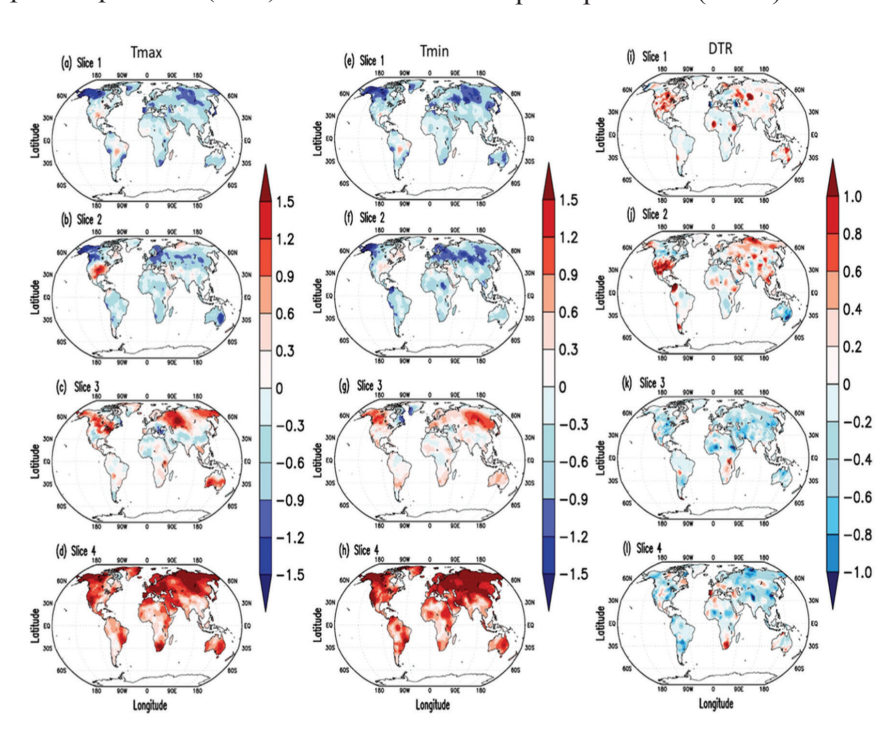


Figure 5: Anomalous change in (a-d) maximum temperature (Tmax), (e-h) minimum temperature (Tmin) and (i-l) diurnal temperature range (DTR) (deg. C) are shown for each time of slices (as composite mean).

pressure (SWVP) are depicted in Figure 3i-l. SWVP shows the water required to saturate the surrounding through evaporation over land. Slice 1 and 2 have shown anomalous negative SWVP indicating a relatively colder world and hence lesser moisture is needed for saturation (Lenderink et al. 2017) (SWVP)(Figure 3i and j). While the anomalous positive SWVP in Slice 3 and 4 reflects an increased water demand and evaporation for saturation in the warming scenario (Figure 3k and 1).

Comparison of the percentage change in the precipitation with the temperature change at each grid point provides an idea about the shift in the precipitation regime with rising temperature (Figure 6a-d). Each dot corresponds to a grid point (Figure 6), which shows that the points are clustered near the centre and spread towards dry-wet and cold-warm regimes. Most of the points in Slice 1 fall near cold-dry and cold-wet regime. Very few points lie in the warm-dry regime (Figure 6a). Slice 2 shows a slight shift towards a relatively warmwet regime (Figure 6b). In Slice 3, most of the points are clustered near the centre and show a relatively warm but inconsistent precipitation regime (Figure 6c). Slice 4 illustrates a high spread of points towards warm and dry/wet regimes, indicating higher global warming in recent times (Figure 6d). Similarly, changes in WVP corresponding to changes in temperature are depicted (Figure 6e-h). In Slice 1, points are scattered in colddry and warm-wet regimes (Figure 6e). However, Slice 2 represents most of the points spreads in the cold-dry regime (Figure 6f). Slice 3 has clustered points near the centre referring to less variation in moisture content in each point (Figure 6g). In Slice 4, an apparent shift towards a warm-wet regime over most of the grid points is evident. The anomalous magnitude of WVP and temperature reaches the maximum value of 2.8 hPa and 4.5°C, respectively (Figure 6h). This confirms that the water holding capacity of the atmosphere has increased under a warming climate. However, precipitation has followed an unpredictable distribution. Most points infer towards a wet-warm condition in the Slices 4 (Figure 6d and h). This is evident that the precipitation intensity has systematic dependence on temperature following the C-C relation.

In Slice 1, a positive relation between precipitation intensity and the temperature is observed in the initial six months of the year, which turns into a negative relationship in the following six months of the year (i.e., returning to the place from where it started) (Figure 7a). A strong positive relationship is found with WVP, in case of temperature rise. The WVP values reach 15.8 hPa as the temperature rises upto 20°C. The path is

reversed while the temperature goes down and follows the same path at a lower temperature. This suggests that the dissipation of the energy distribution while raising the temperature is very much different than the energy distribution due to the cooling process to lower the temperature. Slice 2 has a similar line pattern, but the gap at around 9°C temperature is more than in Slice 1, which suggests lower precipitation with the decrease of temperature (Figure 7a). However, WVP has a similar signature of increasing/decreasing precipitation with temperature rise/fall. WVP pattern follows the C-C relation, while precipitation denies the C-C relation (Lenderink et al., 2017). Therefore, the present study also supports the claim that only the C-C relation cannot be able to explain the precipitation intensity and temperature change relationship (Maeda et al., 2012).

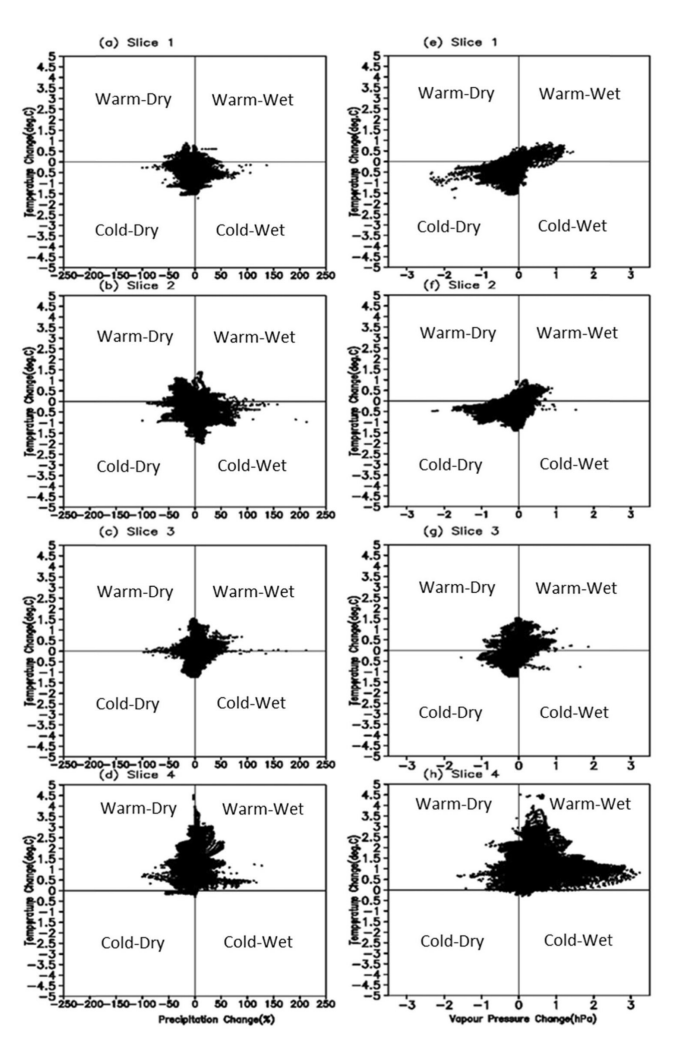


Figure 6: The precipitation change (percentage) and water vapour pressure change with temperature change of each grid points over global land. Figure (a-d) precipitation percentage change vs temperature change and (e-h) water vapour pressure vs temperature change for four slices.

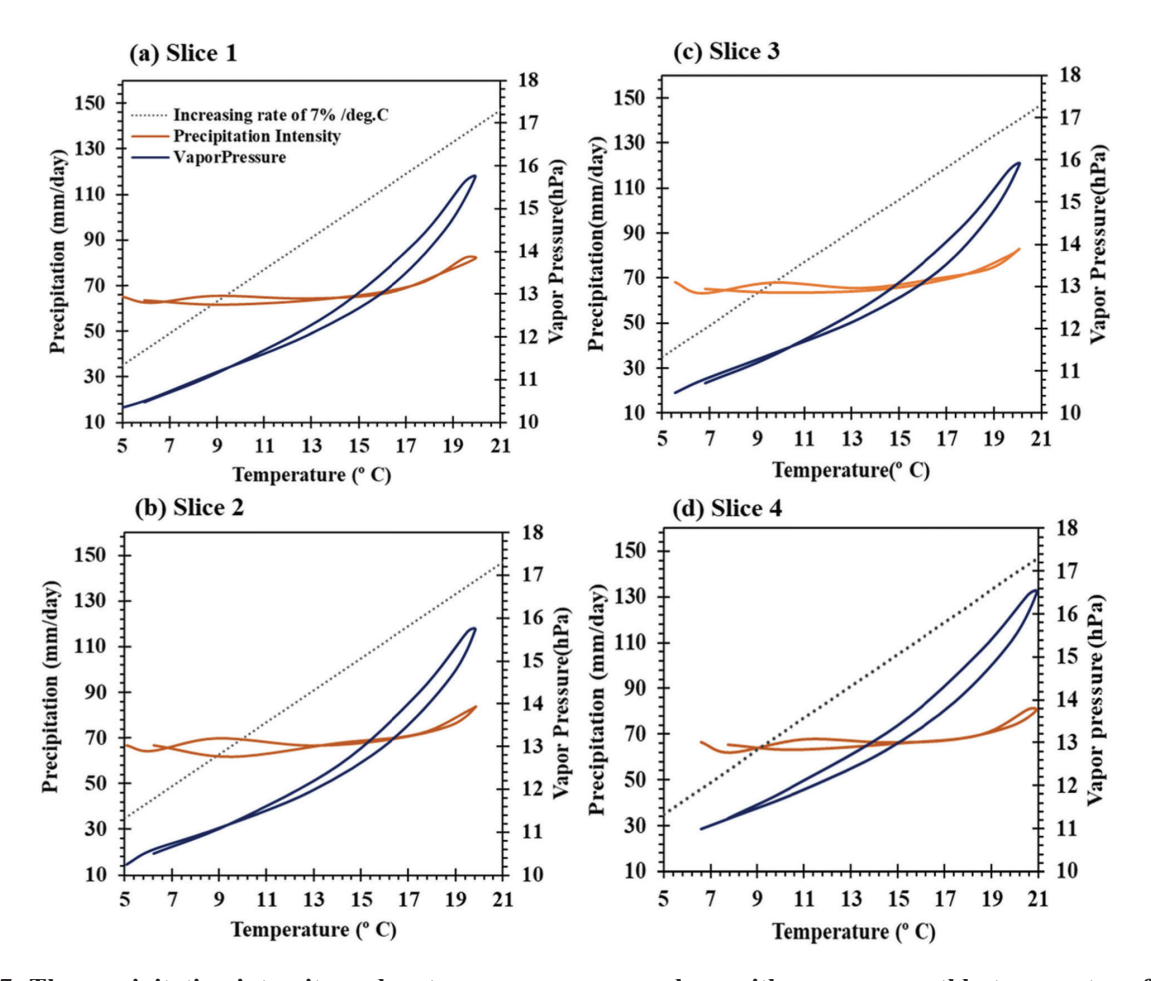


Figure 7: The precipitation intensity and water vapour pressure along with average monthly temperature for each slices (a-d). The dashed line represents increasing rate of 7% /deg. C as Clausius-Clapeyron relation for atmospheric moisture holding capacity.

There is no effect of temperature rise on precipitation until the temperature reaches 17°C or above in all the slices; while beyond 19°C rise in precipitation is a little sharp. The temperature reaches 20°C for Slices 1 to 3 and 21°C for Slice 4 (Figure 7a-d).

The WVP and temperature correlation can be explained by the C-C relation. In all the slices, WVP rises upto 15.8 hPa with the temperature rise upto 20°C with an exception in Slice 4 where WVP rises to 16.5 hPa with temperature rise upto 21°C (Figure 7d). Increasing and decreasing WVP phases intersect each other at 11°C and 11 hPa in all three slices (Slice 1-3), but Slice 4 has an intersection point at 9°C and 11.5 hPa (Figure 7a-d). This clearly indicates the higher water holding capacity of the atmosphere due to global mean air temperature raised by 1°C from the pre-industrial level. Results from the present study clearly distinguish the discrepancy between pre- and post-industrial periods.

The probability distributions of temperature show that the peak of the median values is shifted by approximately 1°C from Slice 1 to 4. The magnitude of the frequency of temperature distribution is also decreased by 0.5% from Slice 1 to 4. The peak in Slice 2 is highest among the slices (Figure 8a). The temperature is rising at a faster rate in the subtropics compared to the tropics (with respect to pre-industrial) (Figure 9a-c). In the case of precipitation, the median values decreased from Slice 1 to 4, and the frequency of the precipitation distribution is decreased from 0.14% to 0.11% (Figure 8b). That suggests the discrete distribution of precipitation in all the slices. The magnitude of the precipitation median has also shifted by 50 mm annually from Slice 1 to 4. The continuously decreasing precipitation trend is observed during the post-industrial period (Figure 9). Moreover, extreme precipitation was observed in the tropics compared to subtropics (Allan et al., 2010) (Figure 10).

Summary

The present study identifies four abrupt temperature and precipitation changes during the study period. The precipitation intensity and temperature changes have deviated from the C-C relation in all the cases. In contrast to this, WVP has followed the C-C relation for all temperature ranges. The recent period has shown abrupt warming amongst all the slices. However, the precipitation has been anomalously low during this period. A decreasing trend in precipitation is found during the post-industrial period over Africa, Eurasia, with an exceptional increase over New Zealand, South America and the eastern U.S.A. A faster rate of increasing temperature is found over subtropics in the post-industrial period (Slice 3 and 4) than in the pre-industrial period (Slice 1 and 2). The anomalously high minimum temperature in Slice 4 over subtropics is observed. Diurnal temperature range (DTR) values suggest anomalous abrupt climatic conditions during Slice 1 to 4. However, DTR is a gauge of climatic variability and instability. The intense anomalous positive nighttime (minimum) temperature is observed in the recent period; which indicates the climate change-induced anomalous high nighttime temperature compared to maximum temperature. The precipitation over the subtropical region is anomalously high as compared to the tropics in recent time. All grid points' climate system (micro-climate) is seen shifting towards warm-wet or warm-dry climate anomalously from past slices to the recent ones. Although the rising temperature has increased the water holding capacity of the atmosphere but does not dictate any distinct precipitation patterns in recent years, which is a plausible cause for most of the abrupt calamity happening in the recent times and increased stress in humankind

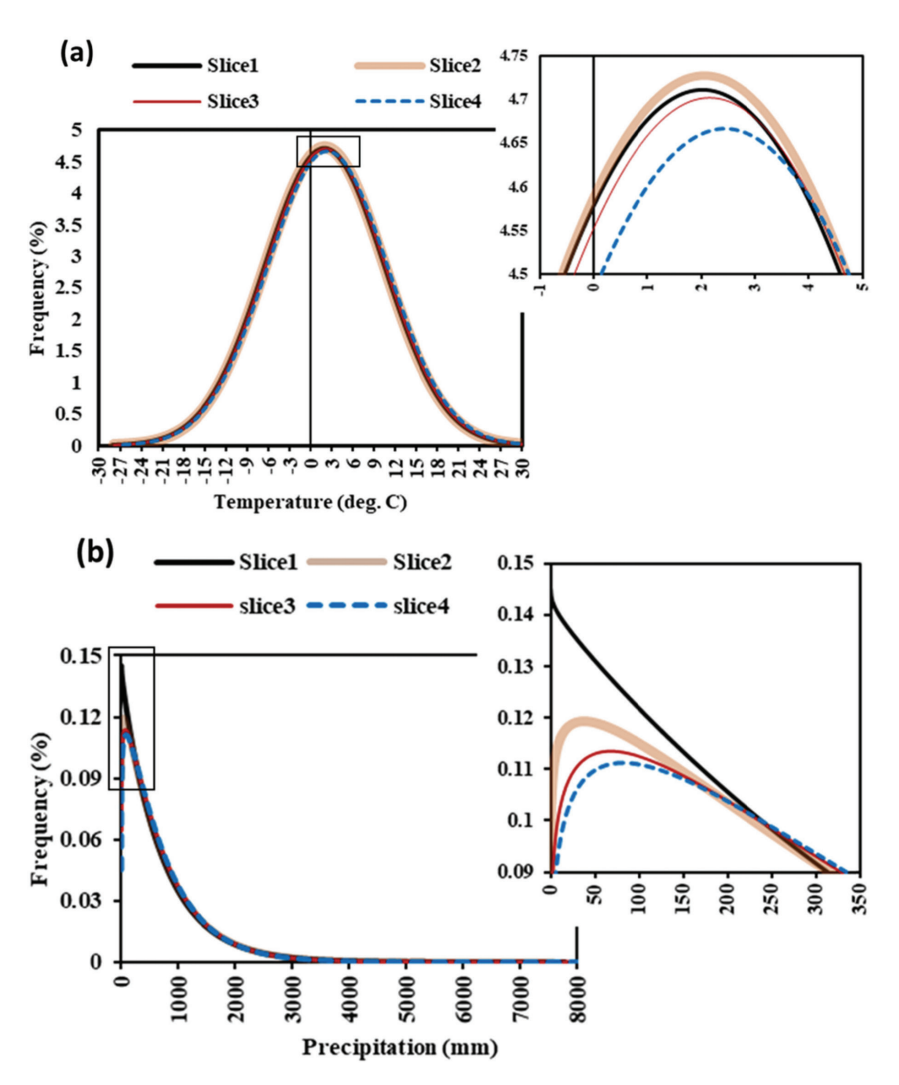


Figure 8: Probability distribution of (a) temperature and (b) precipitation for each time of slices over global land.

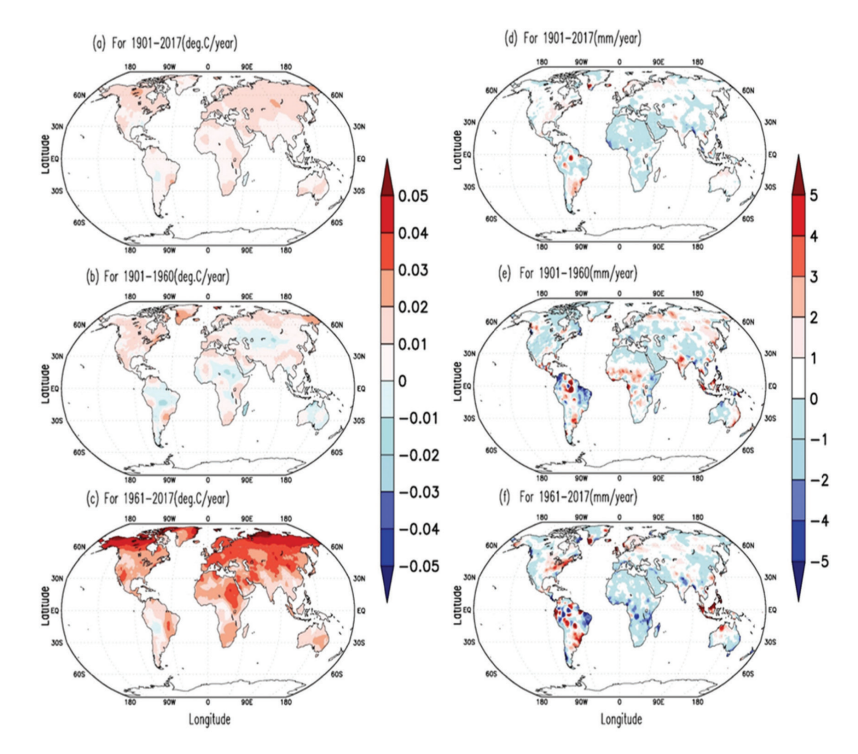


Figure 9: Linear trends of (a-c) temperature and (d-f) precipitation for 1901-2017, 1901-1960: pre-industrial period and 1961-2017: post-industrial period.

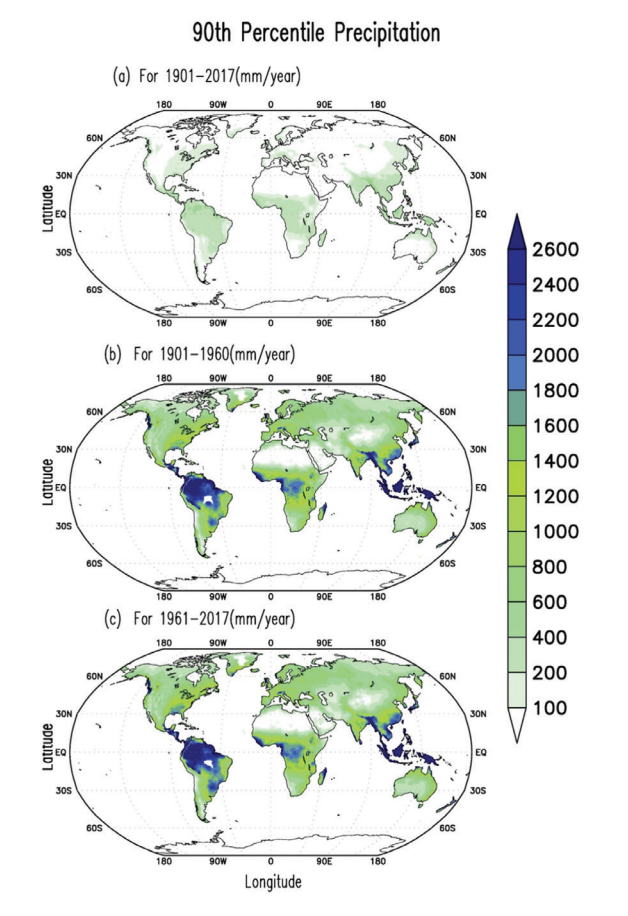


Figure 10: Same as Figure 9, but for the 90th percentile precipitation.

Acknowledgement

The authors highly acknowledge high-resolution CRU dataset free availability. Data used in the present study is taken from CRU and will be archived in the appropriate repository.

Conflict of Interest

There is no competing interests.

Data Availability Statement

Data underlying the findings of the present article can be accessed from Climate Research Unit (CRU)

References

Ahn, C.-H. and Tateishi, R., 1994. Development of global 30-minute grid potential evapotranspiration data set. *Journal of the Japan Society of Photogrammetry and Remote Sensing*, **33:** 12-21.

Allan, R.P., Soden, B.J., John, V.O., Ingram, W. and Good, P., 2010. Current changes in tropical precipitation. *Environmental Research Letters*, **5:** 025205.

Berg, A., Sheffield, J. and Milly, P.C.D., 2017. Divergent surface and total soil moisture projections under global warming. *Geophysical Research Letters*, **44:** 236-244.

- Berg, P., Haerter, J.O., Thejll, P., Piani, C., Hagemann, S. and Christensen, J.H., 2009. Seasonal characteristics of the relationship between daily precipitation intensity and surface temperature. *Journal of Geophysical Research: Atmospheres*, **114**. Available at: https://agupubs.onlinelibrary.wiley.com/doi/abs/10.1029/2009JD012008 [Accessed August 4, 2021].
- Berg, P., Moseley, C. and Haerter, J.O., 2013. Strong increase in convective precipitation in response to higher temperatures. *Nature Geoscience*, **6:** 181-185.
- Booth, B.B.B., Dunstone, N.J., Halloran, P.R., Andrews, T. and Bellouin, N., 2012. Aerosols implicated as a prime driver of twentieth-century North Atlantic climate variability. *Nature*, **484**: 228-232.
- Braganza, K., Karoly, D. and Arblaster, J.M., 2004. Diurnal temperature range as an index of global climate change during the twentieth century. *Geophysical Research Letters*, 31.
- Caesar, J., Alexander, L. and Vose, R., 2006. Large-scale changes in observed daily maximum and minimum temperatures: Creation and analysis of a new gridded data set. *Journal of Geophysical Research: Atmospheres*, 111. Available at: https://agupubs.onlinelibrary.wiley.com/doi/abs/10.1029/2005JD006280 [Accessed August 4, 2021].
- Chen, D. and Dai, A., 2019. Precipitation characteristics in the community atmosphere model and their dependence on model physics and resolution. *Journal of Advances in Modeling Earth Systems*, **11:** 2352-2374.
- Cheng, L., Zhu, J., Abraham, J., Trenberth, K.E., Fasullo, J.T.,
 Zhang, B., Yu, F., Wan, L., Chen, X. and Song, X., 2019.
 2018 Continues record global ocean warming. *Advances in Atmospheric Sciences*, 36: 249-252.
- Davy, R., Esau, I., Chernokulsky, A., Outten, S. and Zilitinkevich, S., 2016. Diurnal asymmetry to the observed global warming. *International Journal of Climatology*, 37.
- Dore, M.H.I., 2005. Climate change and changes in global precipitation patterns: What do we know? *Environment International*, **31:** 1167-1181.
- Easterling, D., Horton, B., Jones, P., Peterson, T., Karl, T.R., Parker, D., Salinger, M., Razuvayev, V., Plummer, N., Jamason, P., et al., 1997. Maximum and minimum temperature trends for the globe. *Science*, **277**: 364-367.
- Grumm, R.H. and Hart, R., 2001. Standardized anomalies applied to significant cold season weather events: Preliminary findings. *Weather and Forecasting*, **16:** 736-754.
- Gu, G., Adler, R., Huffman, G. and Curtis, S., 2007. Tropical rainfall variability on interannual-to-interdecadal and longer time scales derived from the GPCP monthly product. *Journal of Climate*, **20**.
- Haerter, J., Berg, P. and Hagemann, S., 2010. Heavy rain intensity distributions on varying time scales and at

- different temperatures. *Journal of Geophysical Research Atmospheres*, 115.
- Haerter, J.O. and Berg, P., 2009. Unexpected rise in extreme precipitation caused by a shift in rain type? *Nature Geoscience*, **2:** 372-373.
- Hansen, J., Ruedy, R., Sato, M. and Lo, K., 2010. Global surface temperature change. *Reviews of Geophysics*, 48. Available at: https://agupubs.onlinelibrary.wiley.com/doi/ abs/10.1029/2010RG000345 [Accessed August 4, 2021].
- Hansen, J., Sato, M., Ruedy, R., Lo, K., Lea, D.W. and Medina-Elizade, M., 2006. Global temperature change. *Proceedings of the National Academy of Sciences*, 103: 14288-14293.
- Harris, I., Jones, P.D., Osborn, T.J. and Lister, D.H., 2014. Updated high-resolution grids of monthly climatic observations the CRU TS3.10 Dataset. *International Journal of Climatology*, **34:** 623-642.
- Hegerl, G.C., Black, E., Allan, R.P., Ingram, W.J., Polson,
 D., Trenberth, K.E., Chadwick, R.S., Arkin, P.A., Sarojini,
 B.B., Becker, A., et al., 2015. Challenges in quantifying changes in the global water cycle. *Bulletin of the American Meteorological Society*, 96: 1097-1115.
- Held, I. and Soden, B., 2006. Robust responses of the hydrological cycle to global warming. *Journal of Climate*, **19:** 5686-5699.
- Huffman, G., Adler, R., Bolvin, D., and Gu, G., 2009. Improving the global precipitation record: GPCP Version 2.1. *Geophysical Research Letters*, **36**.
- Intergovernmental Panel on Climate Change ed. 2014. Climate Change 2013 The Physical Science Basis: Working Group I Contribution to the Fifth Assessment Report of the Intergovernmental Panel on Climate Change. Cambridge University Press, Cambridge Available at: http://ebooks.cambridge.org/ref/id/CBO9781107415324 [Accessed August 4, 2021].
- IPCC 2018. Global Warming of 1.5°C.An IPCC Special Report on the impacts of global warming of 1.5°C above pre-industrial levels and related global greenhouse gas emission pathways, in the context of strengthening the global response to the threat of climate change, sustainable development, and efforts to eradicate poverty [Masson-Delmotte, V., P. Zhai, H.-O. Pörtner, D. Roberts, J., Skea, P.R., Shukla, A., Pirani, W., Moufouma-Okia, C., Péan, R., Pidcock, S., Connors, J.B.R., Matthews, Y. Chen, X. Zhou, M.I. Gomis, E. Lonnoy, T. Maycock, M. Tignor and T. Waterfield (eds.)]. In Press.
- Jones, R., Westra, S. and Sharma, A., 2010. Observed relationships between extreme sub-daily precipitation, surface temperature, and relative humidity. *Geophysical Research Letters*, 37: 22805.
- Karl, T.R., Kukla, G., Razuvayev, V.N., Changery, M.J., Quayle, R.G., Heim, R.R., Easterling, D.R. and Fu, C.B., 1991. Global warming: Evidence for asymmetric diurnal temperature change. *Geophysical Research Letters*, 18: 2253-2256.

- Lenderink, G., Barbero, R., Loriaux, J. and Fowler, H., 2017. Super-Clausius-Clapeyron scaling of extreme hourly convective precipitation and its relation to large-scale atmospheric conditions. *Journal of Climate*, 30.
- Lenderink, G. and van Meijgaard, E., 2008. Increase in hourly precipitation extremes beyond expectations from temperature changes. *Nature Geoscience*, **1:** 511-514.
- Liu, S.C., Fu, C., Shiu, C.-J., Chen, J.-P. and Wu, F., 2009. Temperature dependence of global precipitation extremes. *Geophysical Research Letters*, **36**. Available at: https://agupubs.onlinelibrary.wiley.com/doi/abs/10.1029/2009GL040218 [Accessed August 4, 2021].
- Lu, J., Sun, G., Mcnulty, S. and Amatya, D.M., 2005. A comparison of six potential evapotranspiration methods for regional use in the Southeastern United States. *JAWRA Journal of the American Water Resources Association*, **41:** 621-633.
- Maeda, E., Utsumi, N. and Oki, T., 2012. Decreasing precipitation extremes at higher temperatures in tropical regions. *Natural Hazards*, **64**.
- Murray, F.W., 1967. On the computation of saturation vapour pressure. *Journal of Applied Meteorology*, **6:** 203-204.
- Osborne, N.S. and Meyers, C.H., 1934. A formula and tables for the pressure of saturated water vapor in the range 0 to 374 C. *Journal of Research of the National Bureau of Standards*, **13**:1.
- Palutikof, J.P., Goodess, C.M. and Guo, X., 1994. Climate change, potential evapotranspiration and moisture availability in the mediterranean basin. *International Journal of Climatology*, **14:** 853-869.
- Peterson, T.C., Karl, T.R., Jamason, P.F., Knight, R. and Easterling, D.R., 1998. First difference method: Maximizing station density for the calculation of long-term global temperature change. *Journal of Geophysical Research: Atmospheres*, **103:** 25967-25974.
- Ramanathan, V., 2001. Aerosols, Climate, and the Hydrological Cycle. *Science*, **294**: 2119-2124.
- Richardson, D., Fowler, H.J., Kilsby, C.G. and Neal, R., 2018. A new precipitation and drought climatology based on weather patterns. *International Journal of Climatology: A Journal of the Royal Meteorological Society*, **38:** 630-648.
- Rosenfeld, D., 2000. Suppression of rain and snow by urban and industrial air pollution. *Science (New York, N.Y.)*, **287**: 1793-1796.
- Rosenfeld, D., Lohmann, U., Raga, G., O'Dowd, C., Kulmala, M., Sandro, F., Reissell, A. and Andreae, M., 2008. Flood or drought: How do aerosols affect precipitation? *Science*, **321:** 1309-1313.

- Scheff, J. and Frierson, D.M.W., 2014. Scaling potential evapotranspiration with greenhouse warming. *Journal of Climate*, **27:** 1539-1558.
- Schuckmann, K., Palmer, M., Trenberth, K.E., Cazenave, A., Chambers, D., Champollion, N., Hansen, J., Josey, S., Loeb, N., Mathieu, P.-P., et al., 2016. An imperative to monitor Earth's energy imbalance. *Nature Climate Change*, 6: 138-144.
- Shenbin, C., Yunfeng, L. and Thomas, A., 2006. Climatic change on the Tibetan Plateau: Potential evapotranspiration trends from 1961-2000. *Climatic Change*, **76**: 291-319.
- SWVP SWVP see at http://www.fao.org/3/X0490E/x0490e07.
- Thorne, P.W., Donat, M.G., Dunn, R.J.H., Williams, C.N., Alexander, L.V., Caesar, J., Durre, I., Harris, I., Hausfather, Z., Jones, P.D., et al., 2016. Reassessing changes in diurnal temperature range: Intercomparison and evaluation of existing global data set estimates. *Journal of Geophysical Research: Atmospheres*, **121:** 5138-5158.
- Trenberth, K., 2011. Changes in precipitation with climate change. Climate Change Research. *Climate Research*, **47:** 123-138.
- Trenberth, K., Dai, A., Schrier, G., Jones, P., Barichivich, J., Briffa, K. and Sheffield, J., 2013. Global warming and changes in drought. *Nature Climate Change*, 4.
- Trenberth, K.E., Dai, A., Rasmussen, R.M. and Parsons, D.B., 2003. The changing character of precipitation. *Bulletin of the American Meteorological Society*, **84:** 1205-1218.
- Trenberth, K.E. and Zhang, Y., 2018. How often does it really rain? *Bulletin of the American Meteorological Society*, **99:** 289-298.
- Tsakiris, G. and Vangelis, H., 2005. Establishing a drought index incorporating evapotranspiration. *European Water*, 9/10
- Wild, M., Ohmura, A. and Makowski, K., 2007. Impact of global dimming and brightening on global warming. *GRL* 34.
- Yang, J., Liu, H.-Z., Ou, C.-Q., Lin, G.-Z., Zhou, Q., Shen, G.-C., Chen, P.-Y. and Guo, Y., 2013. Global climate change: Impact of diurnal temperature range on mortality in Guangzhou, China. *Environmental Pollution*, 175:131-136.
- Yang, S.-E. and Wu, B.-f., 2010. Calculation of monthly precipitation anomaly percentage using web-serviced remote sensing data. *In* 2010 2nd International Conference on Advanced Computer Control pp. 621-625. IEEE, Shenyang, China Available at: http://ieeexplore.ieee.org/document/5486796/ [Accessed August 4, 2021].